Electrocatalysis (2017) 8:288–293
DOI 10.1007/s12678-017-0369-7

ORIGINAL RESEARCH

Direct Butane Utilization on Ni-$(Y_2O_3)_{0.08}(ZrO_2)_{0.92}$-$(Ce_{0.9}Gd_{0.1})O_{1.95}$ Composite Anode-Supported Microtubular Solid Oxide Fuel Cells

Hirofumi Sumi[1] · **Toshiaki Yamaguchi**[1] · **Hiroyuki Shimada**[1] · **Koichi Hamamoto**[1] · **Toshio Suzuki**[1] · **Scott A. Barnett**[2]

Published online: 15 March 2017

Abstract Nickel-yttria-stabilized zirconia-gadolinia-doped ceria (Ni-YSZGDC) composite anodes were investigated to use butane directly for microtubular solid oxide fuel cells (SOFCs). It was confirmed that mechanical mixing and sintering at 1400 °C for the YSZGDC composites resulted in the formation of a YSZ-GDC solid solution. The *n*-butane conversion for the cells with Ni-YSZGDC composite anodes was higher than that with Ni-YSZ anode. However, carbon deposition was observed on the Ni-YSZGDC composite anodes after durability test in *n*-butane. On the other hand, the performance was stable for the cell with the Ni-GDC anode in *n*-butane due to no carbon deposition. The Ni-GDC anode has a high electrochemical activity of carbon oxidation.

Keywords Solid oxide fuel cell (SOFC) · Ni-based anode · Gd-doped ceria · Hydrocarbon · Internal reforming

Introduction

Solid oxide fuel cells (SOFCs) can, in principle, directly use not only hydrogen but also hydrocarbon fuels such as methane and butane.

$$C_xH_{2y} + (2x+y)O^{2-} \rightarrow xCO_2 + yH_2O + (4x+2y)e^- \quad (1)$$

✉ Hirofumi Sumi
h-sumi@aist.go.jp

[1] Inorganic Functional Materials Research Institute, National Institute of Advanced Industrial Science and Technology (AIST), Nagoya, Aichi 463-8560, Japan

[2] Department of Materials Science and Engineering, Northwestern University, Evanston, IL 60208, USA

However, hydrocarbon decomposes into hydrogen and solid carbon at high temperatures.

$$C_xH_{2y} \rightarrow xC + yH_2 \quad (2)$$

Carbon deposition causes rapid deterioration of anode performance due to the deactivation of electrode catalysts and the inhibition of fuel diffusion [1]. Steam reforming of hydrocarbons is generally applied with a steam/carbon (S/C) ratio greater than three in order to prevent carbon deposition.

$$C_xH_{2y} + xH_2O \rightarrow xCO + (x+y)H_2 \quad (3)$$

However, internal reforming of methane at S/C = 3 caused the degradation of Ni-YSZ anodes, because an excess steam oxidized nickel catalysts locally at a vicinity of interface between electrolyte and anode [2]. Therefore, direct hydrocarbon utilization in SOFCs at low S/C ratios is desirable via hydrocarbon reforming, shift reaction, and H_2/CO oxidation electrochemically and thermodynamically.

$$C_xH_{2y} + xO^{2-} \rightarrow xCO + yH_2 + 2xe^- \quad (4)$$

$$CO + H_2O \rightarrow CO_2 + H_2 \quad (5)$$

$$H_2 + O^{2-} \rightarrow H_2O + 2e^- \quad (6)$$

$$CO + O^{2-} \rightarrow CO_2 + 2e^- \quad (7)$$

Murray et al. [3] successfully demonstrated a direct methane SOFC at S/C = 0.03 below 650 °C using a Ni-yttria-doped ceria anode. Park et al. [4] directly used hydrocarbons such as ethane, *n*-butane, 1-butene, and toluene for SOFCs with a Cu-samaria-doped ceria anode at 700 °C. Many researches have been conducted focusing on direct hydrocarbon utilization in SOFCs as reviewed by McIntosh and Gorte [5]. In particular, Cu-based anodes suppress carbon deposition compared to Ni-based anodes during direct hydrocarbon utilization in SOFCs.

However, Cu-based anodes have a lower electrochemical activity of fuel oxidation than Ni-based anodes.

Previously, the authors found that Ni-gadolinia-doped ceria (GDC) anode had high durability on direct butane utilization [6]. A conventional Ni-yttria-stabilized zirconia (YSZ) anode deteriorated rapidly for less than 4 h in butane at S/C = 0.044 and at 610 °C because of a large amount of carbon deposition. The cell with a Ni-GDC anode performed as anode continuously for more than 24 h in butane. Cerium can be reduced from Ce^{4+} to Ce^{3+} under low oxygen partial pressure and high temperature, which causes the suppression of carbon deposition on the Ni-GDC anode in butane at low S/C ratios. On the other hand, Ni-YSZGDC composite anodes have higher electrochemical activity on hydrogen oxidation process [7]. Tetragonal (*t'*) or cubic (*c*) single phase structure is metastable over a wide compositional range for the ZrO_2-CeO_2 solid solutions [8, 9]. Although the O^{2-} ionic conductivity of ZrO_2-CeO_2 solid solutions is lower [10], the electrochemical activity of hydrogen oxidation is higher than that of Ni-YSZ anodes [7, 11].

In the present work, the performance and durability of Ni-YSZGDC composite anode-supported microtubular SOFCs were evaluated under direct butane utilization. The catalytic and electrochemical activities on internal butane reforming and oxidation were investigated by gas chromatography and AC impedance. Carbon deposition behavior was observed with a field emission-scanning electron microscope (FE-SEM) and Raman spectroscopy.

Experimental

Anode microtubes were made from NiO (Sumitomo Metal Mining), $(Y_2O_3)_{0.08}(ZrO_2)_{0.92}$ (YSZ; Tosoh), $(Ce_{0.9}Gd_{0.1})O_{1.95}$ (GDC; Shin-Etsu Chemical), pore former (acrylic resin; Sekisui Plastic), and binder (Cellulose; Yuken Kogyo) powders. The weight ratio of NiO to oxide was 6:4, and the molecular ratios of YSZ to GDC were 100:0 (Ni-100YSZ), 50:50 (Ni-50YSZ50GDC), 25:75 (Ni-25YSZ75GDC), and 0:100 (Ni-100GDC). A pore former of acrylic resin with a grain size of ca. 5 μm was added before sintering to increase anode porosity. These powders were mixed mechanically by kneading machine with adding the proper amount of water for 2 h. The anode microtubes were extruded using a piston cylinder with a metal hole of 2.4 mm (outside diameter) and 1.4 mm (inside diameter). After extrusion, the tubes were dried overnight in air at room temperature. An electrolyte slurry was prepared by mixing YSZ, a binder (polyvinyl butyral; Sekisui Chemical), a dispersant (tallow propylene diamine; Kao), and a plasticizer (dioctyl adipate; Wako Pure Chemical Industries) into ethanol and toluene solvents for 48 h. The YSZ electrolyte was formed by dip-coating. The YSZ thin-film electrolyte and NiO-YSZGDC anode microtube were co-sintered in air for 3 h at 1400 °C. The interlayer of GDC and the cathode of $La_{0.6}Sr_{0.4}Co_{0.2}Fe_{0.8}O_3$-GDC were coated in a similar manner. The weight ratio of LSCF to GDC was 7:3. The GDC interlayer was introduced between the electrolyte and the cathode by using a similar dip-coating method, to prevent chemical reactions between these materials. The interlayer and cathode thin-film layers were sintered sequentially in air for 2 h at 1250 °C and for 1 h at 950 °C, respectively. The outside diameter of microtube was 1.8 mm, and the cathode length was 30 mm after sintering. The thicknesses of the anode, electrolyte, interlayer, and cathode were ca. 400, 5, 1, and 20 μm, respectively. The crystal structures of Ni-YSZGDC powders were evaluated with an X-ray diffractometer (Rigaku RINT-2200) using Cu-Kα radiation at room

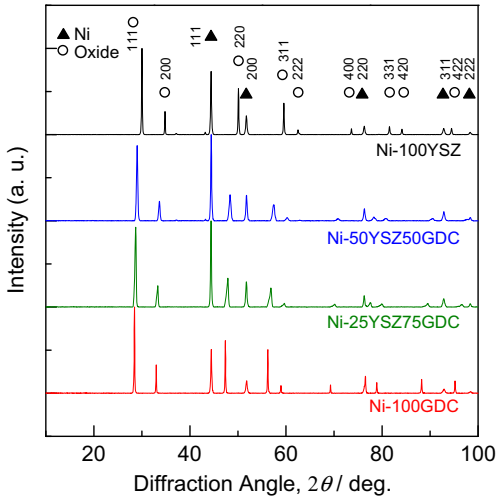

Fig. 1 XRD patterns of Ni-YSZGDC anodes after reduction treatment measured with CuKα radiation

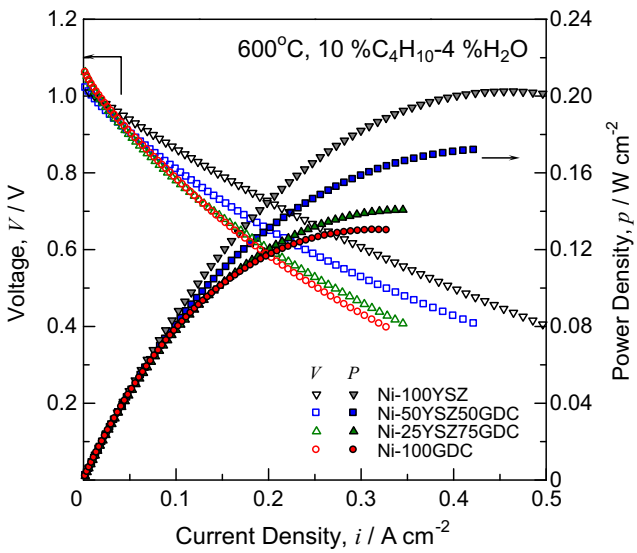

Fig. 2 Current-voltage and power characteristics for the microtubular cells with the Ni-YSZGDC anodes in 10%*n*-C_4H_{10}-4%H_2O-86%N_2 at 600 °C

Table 1 Equilibrium and experimental compositions of reformate gases from 10%*n*-C_4H_{10}-4%H_2O-86%N_2 at 600 °C (H. Sumi et al.)

	Equilibrium		Ni-100YSZ		Ni-50YSZ50GDC		Ni-25YSZ75GDC		Ni-100GDC	
	%	mmol	%	mmol	%	mmol	%	mmol	%	mmol
H_2	30.05	1.799	5.62	0.258	6.81	0.320	8.18	0.398	7.19	0.347
H_2O[a]		0.069		0.119		0.068		0.008		0.000
CO	0.90	0.054	0.83	0.038	1.40	0.066	2.26	0.110	2.28	0.110
CO_2	0.09	0.005	0.23	0.011	0.47	0.022	0.62	0.030	0.72	0.035
CH_4	4.14	0.248	1.55	0.071	2.00	0.094	2.95	0.144	2.85	0.138
n-C_4H_{10}	0.00	0.000	8.27	0.380	7.77	0.366	7.12	0.347	7.44	0.359
N_2	64.82	3.884	83.51	3.839	81.55	3.839	78.86	3.839	79.51	3.839
C(s)		1.478								
conv.	100		17.3		22.3		28.8		25.6	
C		1.79		1.64		1.65		1.67		1.72
H		4.82		4.84		4.81		4.86		4.84
O		0.18		0.18		0.18		0.18		0.18

[a] The concentration of H_2O was not measured, and the molecular amount of H_2O was estimated in consideration for mass balance of oxygen species

temperature in air. The specific surface area of Ni catalyst in Ni-YSZGDC anodes was ca. 6 $\mu m^2/\mu m^3$ which was derived from 3D microstructural analysis by focus ion beam (FIB)-SEM observation in the previous report [7].

The NiO-YSZGDC anodes were reduced for 2 h at 600 °C in 20%H_2-4%H_2O-76%N_2 before electrochemical evaluation. Then, a mixture of 10%*n*-C_4H_{10}-4%H_2O-86%N_2 (S/C = 0.10) was supplied as fuel at a flow rate of 100 mL/min to the anode (inside), and the air was supplied as oxidant at 100 mL/min to the cathode (outside). The composition of exhaust gas from the anode was analyzed with a thermal conductivity detector (TCD) in a micro gas chromatography (Agilent Technologies 490; H_2, N_2, CH_4, CO: Molecular Sieve 5A column with Ar as a carrier gas, CO_2, C2, C3, C4: PoraPLOT Q column with He as a carrier gas). The characteristics of power generation and AC impedance were evaluated with a potentiostat/galvanostat built in an impedance analyzer (Autolab PGSTAT302). Platinum paste TR-7905 (Tanaka Kikinzoku Kogyo) was used as a current collector on the LSCF-GDC cathode [12]. Current-voltage (*i-V*) characteristics were measured from open circuit voltage (OCV) to 0.4 V at a sweep rate of 5 mV/s. The AC impedance was measured at OCV in the frequency range from 1 MHz to 0.1 Hz with 20 steps per logarithmic decade. After durability tests at 0.15 A/cm^2 and 600 °C in 10%*n*-C_4H_{10}-4%H_2O-86%N_2, deposited carbon on Ni-YSZGDC anodes was observed with FE-SEM (JEOL JSM-6330F) and Raman spectroscopy (Horiba XploRA).

Results and Discussion

Figure 1 shows the X-ray diffraction (XRD) patterns of the reduced Ni-YSZGDC powders measured with CuKα radiation at room temperature in air. The XRD patterns of the Ni-100YSZ and Ni-100GDC consisted of a face-centered cubic nickel and a fluorite-type tetragonal YSZ or cubic GDC. The lattice parameters of Ni, YSZ, and GDC were 0.3522, 0.5138, and 0.5419 nm, respectively. The diffraction peaks of YSZ and GDC were not separated for the Ni-50YSZ50GDC and Ni-25YSZ75GDC. While the lattice parameter of nickel was unchanged by the substitution of GDC with YSZ, that of YSZGDC increased linearly with GDC content agreeing with Vegard's law. This means that the mechanical mixing and sintering at 1400 °C for the Ni-YSZGDC composites resulted in the formation of a YSZ-GDC solid solution.

Figure 2 shows the current-voltage (*i-V*) and current-power (*i-p*) characteristics for the anode-supported microtubular SOFCs in 10%*n*-C_4H_{10}-4%H_2O-86%N_2 at 600 °C. The theoretical electromotive force (EMF) is 1.13 V at 600 °C. However, the experimental OCVs were 1.02–1.07 V in the present work. It suggests that the composition of reformate

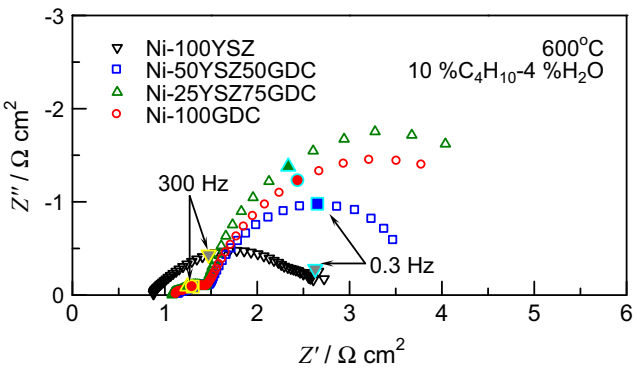

Fig. 3 AC impedance spectra for the microtubular cells with the Ni-YSZGDC anodes in 10%*n*-C_4H_{10}-4%H_2O-86%N_2 at 600 °C measured between the anode and cathode under OCV state

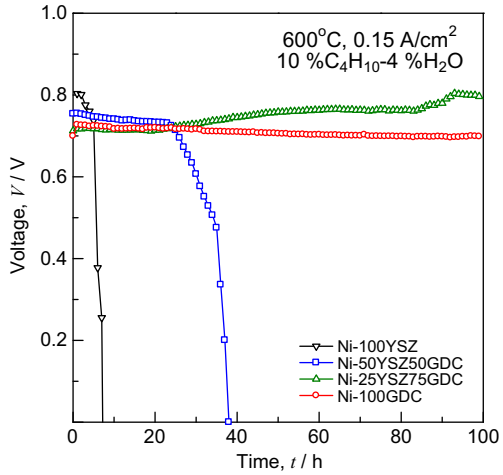

Fig. 4 Voltage at 0.15 A/cm^2 as a function of time for the microtubular cells with the Ni-YSZGDC anodes in 10%*n*-C_4H_{10}-4%H_2O-86%N_2 at 600 °C

gases did not reach an equilibrium state at a fuel flow rate of 100 mL/min for microtubular cells with 1.8 mm in diameter. Table 1 shows the equilibrium and experimental compositions of reformate gases from 10% *n*-C_4H_{10}-4%H_2O-86%N_2 (*n*-C_4H_{10}: 0.446 mmol, H_2O: 0.179 mmol, N_2: 3.839 mmol) at 600 °C under OCV state. The percentage of H_2O is not included in Table 1, because H_2O was removed by vapor condenser before gas sampling. The molecular amount of H_2O is estimated in consideration for mass balance of oxygen species. In the equilibrium, the *n*-butane is decomposed into H_2, CH_4, and solid carbon (C(s)), and the conversion should be about 100%. However, the experimental conversion was only 17–29% due to insufficient space velocity in the present work. The conversion of Ni-25YSZ75GDC was maximum. The products of H_2 and CH_4 were proportional to the *n*-butane conversion for all anodes. On the other hand, CO and CO_2 were produced more than expected in equilibrium. The products of CO and CO_2 increased with increasing GDC content for Ni-YSZGDC anodes. The total carbon mass in the exhaust gas was smaller than that in the input *n*-butane (1.79 mmol), which means the occurrence of carbon deposition in OCV state. The difference in total carbon mass between the input and exhaust gases is minimum for Ni-100GDC.

Figure 3 shows the AC impedance spectra for the microtubular cells with the Ni-YSZGDC anodes in 10%*n*-C_4H_{10}-4%H_2O-86%N_2 at 600 °C measured between the anode and cathode under OCV state. The impedance arcs at high frequency for the anode containing GDC were smaller than those for Ni-100YSZ. The similar behavior was previously observed in hydrogen fuel [7]. It was previously confirmed that the impedance at 0.1–1 kHz was due to fuel oxidation process for anode-supported microtubular SOFCs [13]. The electrochemical activity of fuel oxidation for the anode containing GDC is higher than that of Ni-100YSZ. On the other hand, the impedance at low frequency adheres to the following sequence: Ni-100YSZ < Ni-50YSZ50GDC < Ni-100GDC < Ni-25YSZ75GDC. This sequence is the same as *n*-butane conversion. The internal reforming of *n*-butane increased the impedance at low frequency.

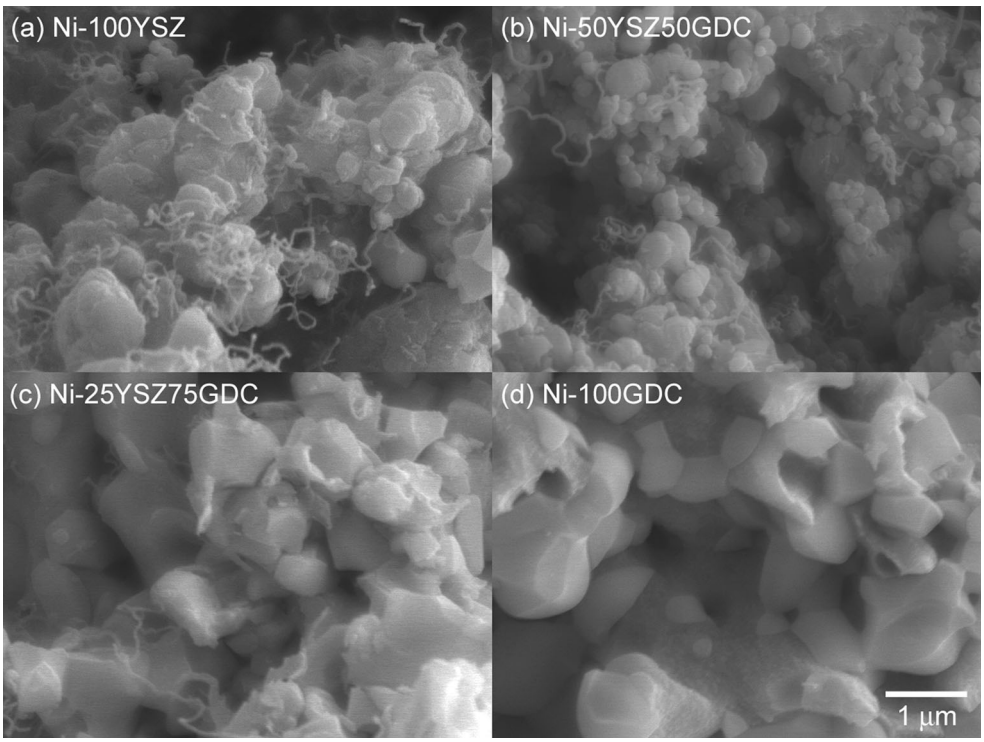

Fig. 5 Scanning electron microscopic images of Ni-YSZGDC anodes after the durability test in 10%*n*-C_4H_{10}-4%H_2O-86%N_2 at 600 °C

Figure 4 shows the voltage at 0.15 A/cm^2 as a function of time for the microtubular cells with the Ni-YSZGDC anodes in 10%*n*-C_4H_{10}-4%H_2O-86%N_2 at 600 °C. The voltage dropped rapidly to less than 0 V after 7 h for Ni-100YSZ. After the durability test, deposited carbon was coated on the Ni catalysts, and many carbon nanofibers grew up from the Ni catalysts in Ni-100YSZ as shown in Fig. 5a. The voltage decreased gradually to less than 0 V after 38 h for Ni-50YSZ50GDC. Carbon deposition was also confirmed for Ni-50YSZ50GDC after the durability test as shown in Fig. 5b. On the other hand, power can be generated continuously over a period of 100 h for Ni-25YSZ75GDC and Ni-100GDC. Figure 6 shows the Raman spectra for Ni-YSZGDC anodes after the durability test in 10%*n*-C_4H_{10}-4%H_2O-86%N_2 at 600 °C. The peaks at ca. 460 and 620 cm^{-1} are ascribed to an F_{2g} band of ceria and an E_g band of zirconia, respectively. The intensity was normalized in consideration of YSZ/GDC ratio [14]. For Ni-100YSZ, Ni-50YSZ50GDC, and Ni-25YSZ75GDC, the peaks were also observed at ca. 1350 and 1580 cm^{-1}, which are ascribed to D (amorphous carbon) and G (graphite) bands, respectively [15–18]. The peak intensity decreased with increasing GDC content. The intensity ratios of G to D bands were 3.0, 2.7, and 2.6 for Ni-100YSZ, Ni-50YSZ50GDC, and Ni-25YSZ75GDC, respectively. The increase in voltage for Ni-25YSZ75GDC was caused by a small amount of the deposition of graphite, which has high electronic conductivity. However, the Ni-25YSZ75GDC might deteriorate over a period of several-hundred h under direct butane utilization, because increasing the amount of deposited carbon causes catalytic deactivation for fuel oxidation. For Ni-100GDC, the voltage was stable over a period of 100 h under direct butane utilization, and no carbon deposition was observed by SEM and Raman spectroscopy after the durability test. Although the *n*-butane conversion for Ni-100GDC was lower than that for Ni-25YSZ75GDC as shown in Table 1, the difference in total carbon mass between the input and exhaust gases is minimum for Ni-100GDC. The amount of deposited carbon was slight in OCV state, and the electrochemical oxidation of carbon easily occurred by current loading at 0.15 A/cm^2 for Ni-100GDC. The Ni-GDC anode has high durability against direct butane utilization.

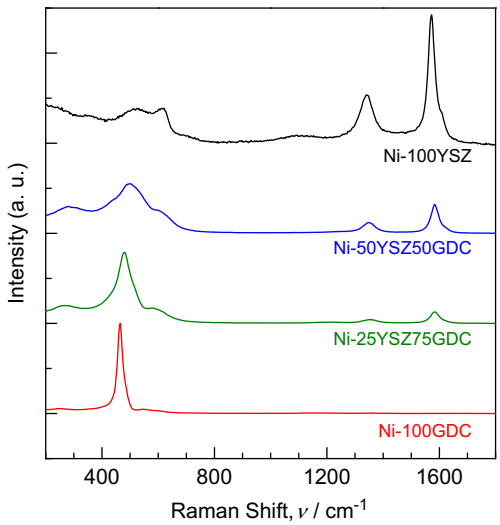

Fig. 6 Raman spectra for Ni-YSZGDC anodes after the durability test in 10%*n*-C_4H_{10}-4%H_2O-86%N_2 at 600 °C

Conclusion

In the present work, the performance and durability of Ni-YSZGDC composite anode-supported microtubular SOFCs were evaluated under direct butane utilization. The experimental OCV was lower than the theoretical EMF due to low *n*-butane conversion. The conversion for Ni-25YSZ75GDC was maximum. Power can be generated continuously over a period of 100 h for Ni-25YSZ75GDC and Ni-100GDC. However, slight carbon deposition was observed by FE-SEM and Raman spectroscopy for Ni-25YSZ75GDC after direct butane utilization. For Ni-100GDC, no carbon deposition was observed after the durability test, because the difference in total carbon mass between the input and exhaust gases was minimum for Ni-100GDC. Ni-YSZGDC composite anode has a high catalytic activity of fuel reforming, and Ni-GDC anode has a high electrochemical activity of carbon oxidation.

References

1. K. Eguchi, H. Kojo, T. Takeguchi, R. Kikuchi, K. Sasaki, Solid State Ionics **152–153**, 411 (2002)
2. H. Sumi, T. Yamaguchi, T. Suzuki, H. Shimada, K. Hamamoto, Y. Fujishiro, Electrochem. Commun. **49**, 34 (2014)
3. E.P. Murray, T. Tsai, S.A. Barnett, Nature **400**, 649 (1999)
4. S.D. Park, J.M. Vohs, R.J. Gorte, Nature **404**, 265 (2000)
5. S. McIntosh, R.J. Gorte, Chem. Rev. **104**, 4845 (2004)
6. H. Sumi, T. Yamaguchi, K. Hamamoto, T. Suzuki, Y. Fujishiro, J. Power Sources **220**, 74 (2012a)
7. H. Sumi, D. Kennouche, K. Yakal-Kremski, T. Suzuki, S.A. Barnett, D.J. Miller, T. Yamaguchi, K. Hamamoto, Y. Fujishiro, Solid State Ionics **285**, 227 (2016)
8. E. Tani, M. Yoshimura, S. Somiya, Revised phase diagram of the system ZrO_2-CeO_2 below 1400 °C. J. Am. Ceram. Soc. **66**, 506 (1983)
9. M. Yashima, H. Arashi, M. Kakihana, M. Yoshimura, J. Am. Ceram. Soc. **77**, 1067 (1994)
10. A. Tsoga, A. Naoumidis, D. Stover, Solid State Ionics **135**, 403 (2000)
11. H. Takahashi, T. Takeguchi, N. Yamamoto, W. Ueda, Solid State Ionics **185**, 52 (2011)
12. H. Sumi, T. Yamaguchi, K. Hamamoto, T. Suzuki, Y. Fujishiro, J. Electrochem. Soc. **160**, F1232 (2013)
13. H. Sumi, T. Yamaguchi, K. Hamamoto, T. Suzuki, Y. Fujishiro, T. Matsui, K. Eguchi, Electrochim. Acta **67**, 159 (2012b)

14. N.M. Sammes, G.A. Tompsett, Z. Cai, Solid State Ionics **121**, 121 (1999)
15. H. Sumi, Y.-H. Lee, H. Muroyama, T. Matsui, K. Eguchi, J. Electrochem. Soc. **157**, B1118 (2010)
16. H. Sumi, Y.-H. Lee, H. Muroyama, T. Matsui, M. Kamijo, S. Mimuro, M. Yamanaka, Y. Yakajima, K. Eguchi, J. Power Sources **196**, 4451 (2011a)
17. H. Sumi, P. Puengjinda, H. Muroyama, T. Matsui, K. Eguchi, J. Power Sources **196**, 6048 (2011b)
18. Y.-H. Lee, H. Sumi, H. Muroyama, T. Matsui, K. Eguchi, J. Electrochem. Soc. **160**, F579 (2013)